Microelectronics Reliability 53 (2013) 452–462

Contents lists available at SciVerse ScienceDirect

Microelectronics Reliability

journal homepage: www.elsevier.com/locate/microrel

Mechanical assessment of an anisotropic conductive adhesive joint of a direct access sensor on a flexible substrate for a swallowable capsule application

P. Jesudoss [a,*], A. Mathewson [a,1], W.M.D. Wright [b,2], F. Stam [a,1]

[a] Tyndall National Institute, Lee Maltings, Prospect Row, Cork, Ireland
[b] Department of Electrical and Electronic Engineering, University College Cork, Cork, Ireland

ARTICLE INFO

Article history:
Received 25 June 2011
Received in revised form 26 September 2012
Accepted 27 September 2012
Available online 10 November 2012

ABSTRACT

Sensor interconnection achieved with Flip Chip (FC) technology and most particularly with Anisotropic Conductive Adhesive (ACA) is a very attractive technique, in achieving a Direct Access Sensor (DAS), in a swallowable diagnostic sensing capsule. This paper describes the work carried out to mechanically characterise the ACA joints when they are inserted in the capsule to determine the smallest capsule diameter that could be used without imparting excessive stress on the interconnect in the DAS integration process for a specific substrate and chip design. Three point inward bending was used to study the effect of the mechanical loading on the joints during the insertion process. The results showed that the insertion force linearly increased and leveled off at a, low friction, constant value. The spring constant of the linear region in a 23 mm was 0.2729 N/mm and increased to 1.5 N/mm for the 15 mm diameter hole. It showed that the spring constant decreased linearly as the diameter increased, signifying that for the same distance, less force will be required in a larger diameter hole than in the small diameter holes. During insertion the stress in the assembly, was higher towards the centre of the chip and the window than at the edge of the chip and the ACA fillet. This was characterised by it exhibiting lower voltage values measured in the partial daisy chains that were close to the window rather than the ones that were situated away from the window. The insertion test suggested that the 23 mm diameter hole would be the smallest suitable hole for insertion of this assembly. Failure analysis revealed that the depression and the wide crack close to the window imply that the stress was high in this region. The cross sectional analysis showed that failure occurred within silicon/silicon chip pad and that the ACA contacts form a strong joint and was able to withstand the insertion force required to secure the ACA sensor in place before encapsulation.

1. Introduction

With recent advances in microelectronics, wireless communication and sensor development, the limitations of endoscopy is overcome in the format of a biomedical swallowable capsule [1]. The swallowable capsule is an autonomous system which contains a sensor, the associated electronics for signal conditioning and amplifying and a radio transmitter, all encapsulated in a biocompatible material. The swallowable capsule is based on a non-invasive technique which can provide information about the whole gastrointestinal (GI) tract. The concept of the first radio telemetry ingestible capsule was put forward by Mackay and Jacobson in 1957 [1,2]. Swallowable capsules can be classified into families of imaging capsules (PillCam, Olympus Optical) [2–4], drug delivery systems [2,4,5] and sensing capsules [1,2,4–12]. Unlike imaging and drug delivery capsules where none of the parts are exposed, chemical sensing capsules have one or more sensors that can measure biochemical variables related to the gut ecosystem through exposed sensors. But in none of the diagnostic sensing capsules is the sensor attachment (the first level packaging of the sensor in a swallowable capsule) is achieved through Flip Chip (FC), and in particular by the Flip Chip Over Hole (FCOH) method using Anisotropic Conductive Adhesive (ACA).

ACAs relatively simple process steps [13] make it suitable for bonding a Direct Access Sensor (DAS). In a DAS, ACA not only provides the electrical interconnection to the sensing die but simultaneously seals the interconnect area around the die and the flexible substrate. This sealing should provide protection to the underlying electronics in a capsule application, as shown in Fig. 1.

During DAS integration into a swallowable capsule, a mechanical force is required to push the sensor assembly through the length of the capsule before securing the chip and the substrate in the capsule for the encapsulation process [14]. The compressive force during the securing of the chip used in this study has been shown to be 7 N [14]. This study also showed that the DAS packaging was reliable (as the electronic functionality and chemical

* Corresponding author. Tel.: +353 214904142.
E-mail addresses: pio.jesudoss@gmail.com (P. Jesudoss), alan.mathewson@tyndall.ie (A. Mathewson), bill.wright@ucc.ie (W.M.D. Wright).
[1] Tel.: +353 214904142.
[2] Tel.: +353 214902213.

0026-2714/$ - see front matter © 2012 Elsevier Ltd. All rights reserved.
http://dx.doi.org/10.1016/j.microrel.2012.09.014

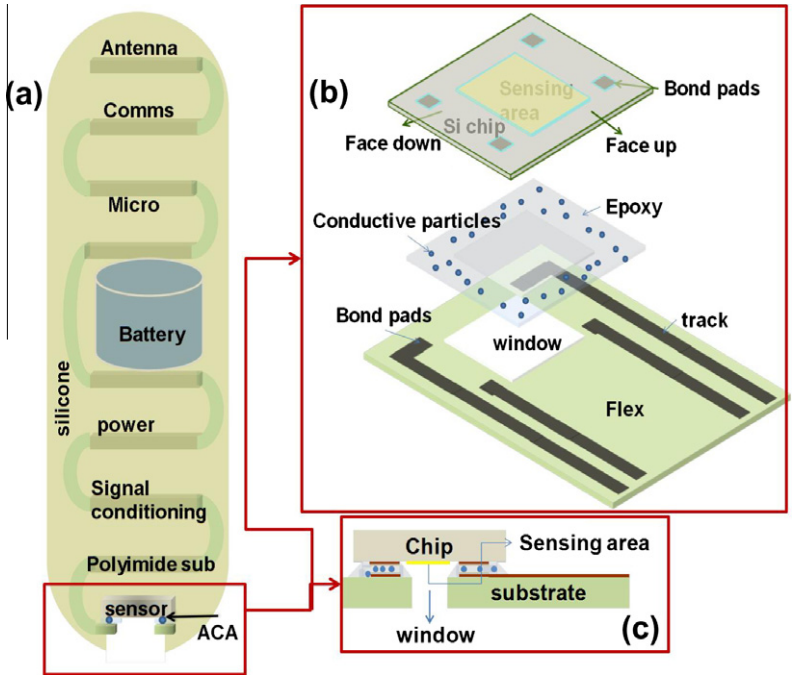

Fig. 1. Schematic of (a) capsule with (b) expanded image of FCOH/DAS and (c) cross sectional view of FCOH/DAS interconnections based on ACA.

sensing performance was not compromised) and that the mechanical securing did not degrade the ACA joints. But it did not provide any information about the joint behaviour during the capsule insertion process.

Fig. 2a and b shows the three point bending and four point bending tests [15–19] that are often used to assess the mechanical reliability of ACA joints. Depending on the position of the die on the substrate and the *z* axis, the bending could be classified into two categories [20,21]: (i) the outward bend characterised by the die positioned on the negative part of the *z* axis as shown in Fig. 2a and b and (ii) the inward bend distinguished by the die positioned on the positive side of the *z* axis, Fig. 3.

Most of the literature deals with outward bending using three or four point bending. A study conducted by Rizvi et al. [15] on the outward three point bending on the ACF joint behaviour showed that the stresses were high on the corners where the chip and ACF were connected together. The high stress at the corners led to increased ACF thickness at the corners and eventually caused a greater gap between the chip and the substrate at the corner positions and the failure of the corner joints.

Cai et al. [20,21] reported on the reliability evaluation of a flexible RFID tag using ACA. The flexibility reliability test showed that the outward bend was more destructive on the contact conductivity than the inward bend. It was concluded that the outward bend caused a tearing effect and that the bend cycle caused the particles between the bump and the pad to undergo an open–close action. Furthermore the inward bending created a constant compressive stress on the ACA joints providing a stable contact resistance during the test.

The DAS capsule integration of the FCOH sensor assembly in this work could be only achieved by an inward bending of the sensor assembly. This paper describes the work carried out to mechanically characterise the ACA joints during the capsule insertion process and to determine the smallest capsule diameter that could be used without imparting excessive stress on the interconnect in the DAS integration process for a specific substrate and chip design. It will investigate the forces required for the insertion of the flex assembly (fixed size) into different sized capsules. The following section describes the materials and the method used for the research. This is followed by the ACA assembly insertion test into different diameter holes to determine the smallest diameter that could be safely used for a specific assembly.

2. Materials and method

2.1. Test chip

The test chip was a 5 mm × 5 mm silicon die with a thickness of 0.5 mm. The test chip was designed specifically for this FC reliability investigation and had an array of 144 (100 μm × 100 μm) pads, with a pad pitch of 400 μm, as shown in Fig. 4. An interleaved sequence of connective pads was laid out on the chip so that it could be used as a daisy chain in the final assembly and thus monitor the

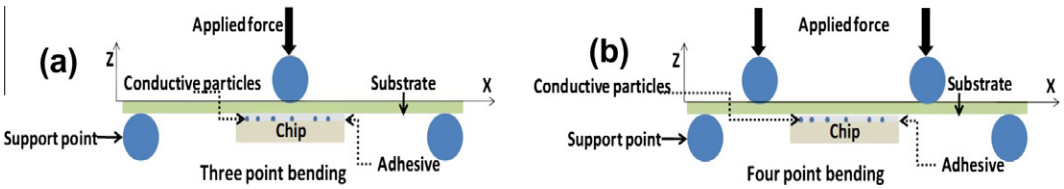

Fig. 2. Schematic of (a) three point; and (b) four point outward bending, force applied to substrate.

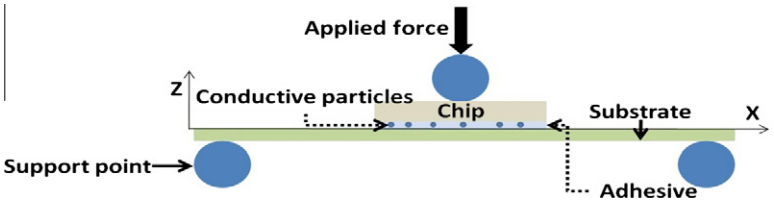

Fig. 3. Schematic of three point inward bending, force applied to chip.

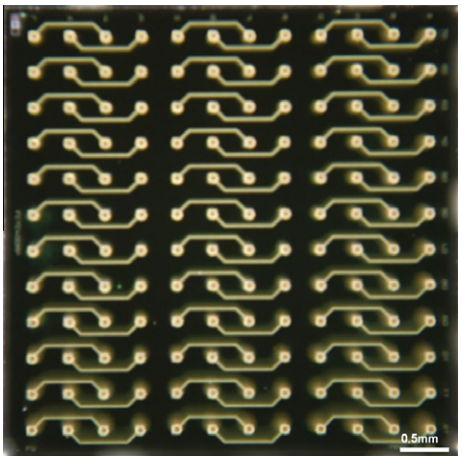

Fig. 4. Micrograph of test chip with coined gold stud bumps.

continuity of the flip chip joints during the mechanical insertion of the assembly. The unbumped die had an aluminium pad metallization. The die was then gold (Au) stud bumped and coined. The height of the coined stud bump was around 40 μm. The main purpose of the coined stud bump was to maximise the contact area during bonding.

2.2. Flex substrate

Fig. 5a shows the Protel layout of the flex substrate. It was 8 cm × 8 cm single sided flex in the form of a cross. In the centre of the cross, at around 4 cm from the edge of the cross, a 2.4 mm window was laser cut to expose the centre of the chip to the surrounding environment as shown in Fig. 5a. At around 3.3 cm from the four edges of the cross, slits with circular edges of radius 0.95 mm were cut to facilitate the folding of the flexible substrate during the encapsulation process. The conducting tracks on the board were terminated with a connector pad which had 2 mm holes to enable soldering of wires to carry out electrical testing. The thickness of the flex substrate was 0.1 mm. The copper tracks on the flexible substrate were 15 μm thick while on the substrate bond pads, an additional 5 μm Ni and 0.05 μm of electroplated flash gold were deposited. Fig. 5b shows the manufactured flexible substrate while Fig. 5c shows the alternating conductive lines for the daisy chain measurement. The sensor interconnection part of the test structure resembles the DAS structure used in the sensor assembly. The overall difference of this test structure to Fig. 1 sensor assembly is the foldable arms that were designed to monitor the joint performance during the insertion process. The foldable arms made the test structure wider in comparison to the actual sensor assembly.

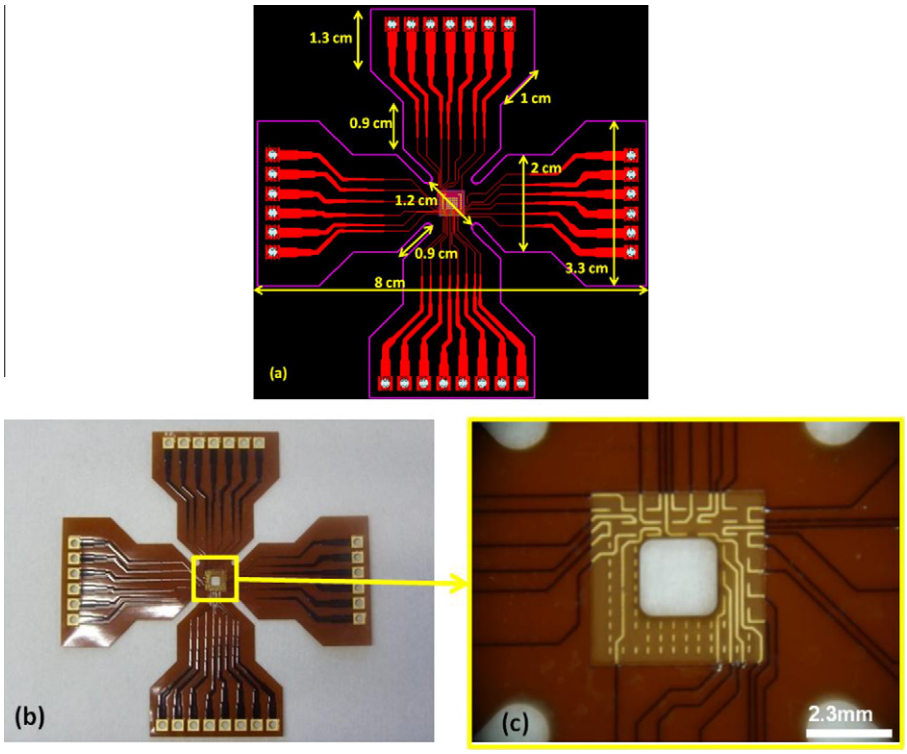

Fig. 5. (a) Protel layout of the flex substrate, (b) micrograph of the flex substrate; and (c) micrograph detail showing conductive lines for daisy chain measurement.

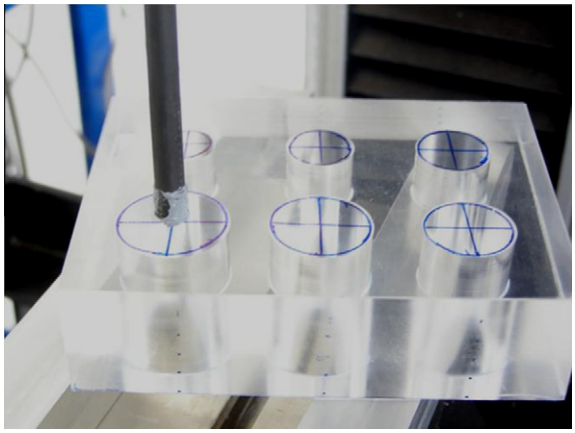

Fig. 6. Polycarbonate block with different diameter holes.

2.3. Bonding process

FP5300 ACA from Henkel was used for bonding the chip to the substrate. The ACA was dispensed on the board using a CAM/ALOT 1414 liquid dispense system. Dots were dispensed close to the bond pads and alignment and bonding of the chip/substrate was performed using a Finetech Flip-Chip bonder. Bonding was carried out at a ramp rate of 2 °C/s with a hold at 180 °C for 40 s and a cool down rate at 3 °C/s and with a bonding pressure of 69 MPa, calculated for the total surface of the Au bumps on the bond pads, for 8 s. These bonding process settings are comparable to the known bonding setting [22,23]. The average bond line thickness of the adhesive taken from 10 samples was approximately 21 μm with a tolerance of 1 μm.

2.4. Assembly insertion test

Fig. 6 shows a polycarbonate block of 75 mm × 100 mm × 27 mm in which 23 mm, 21 mm, 19 mm, 17 mm, 15 mm and 13 mm diameter through holes were drilled to carry out the mechanical testing. These holes represent different diameter capsules. Due to the fact that the diagonal slits on the flex board had a length of 12 mm diameter, the minimum diameter hole was set at 13 mm.

In order to carry out the mechanical testing the ACA assembly had to be placed on top of each hole and then pushed through. An 11 mm diameter iron rod with its tip covered in 1 mm of silicone was used as a pushing tool. Before each test, the pushing tool and the ACA assembly were placed in the centre of each hole with the hole diameter becoming progressively smaller. This was carried out to ensure that the assembly went down the middle of each hole.

After centreing the rod and the ACA assembly, the mechanical test was carried out by placing the iron rod directly on the middle of the back of the chip and pushing the assembly though the hole. Unlike three or four point bending where the end of the substrate is clamped, the substrate was free to go through the hole. Fig. 7 shows the mechanical test setup and the electrical setup that was used for testing the ACA joints during capsule insertion. Since the die was positioned on the positive side of the z axis, this setup could be classified as an inward bending process. The mechanical test was carried out on Instron 5565 with a cross head speed of 2 mm/min, and the required insertion force was recorded. All the mechanical tests were performed at room temperature with a relative humidity (RH) of 50%.

2.5. Electrical testing

Fig. 8a and b shows the schematic of the test assembly and the electrical test setup that was used to record the electrical behaviour of the assembly during the mechanical test. Fig. 8b shows the daisy chain layout that was used in the electrical testing. A preliminary evaluation of the design showed that the test structure was symmetric in nature. Therefore due to the symmetry of the assembly only half of the assembly was considered for electrical characterisation to simplify the test and reduce the amount of data. As shown in Fig. 8, the test assembly contained four partial daisy chains defined as $x1$, $x2$, $x3$ and y and a total daisy chain z (all four daisy chains connected together). Three partial daisy chains were positioned in the x direction while one was positioned in the y direction. The partial daisy chain $x1$ was located 1 mm from the window, $x2$ was located 0.6 mm from the window, $x3$ was located 0.2 mm from the window and y was located at 0.2 mm from the window. In order to electrically assess the joints a four point measurement was devised by applying a constant current of 100 μA to the total daisy chain while the voltage was measured at the total daisy chain and the partial daisy chains $x1$, $x2$, $x3$ as shown in Fig. 8. As the electrochemical measurements showed that the current that passed through the joint was in the range of microamps, 100 μA was used in the four point electrical measurement test.

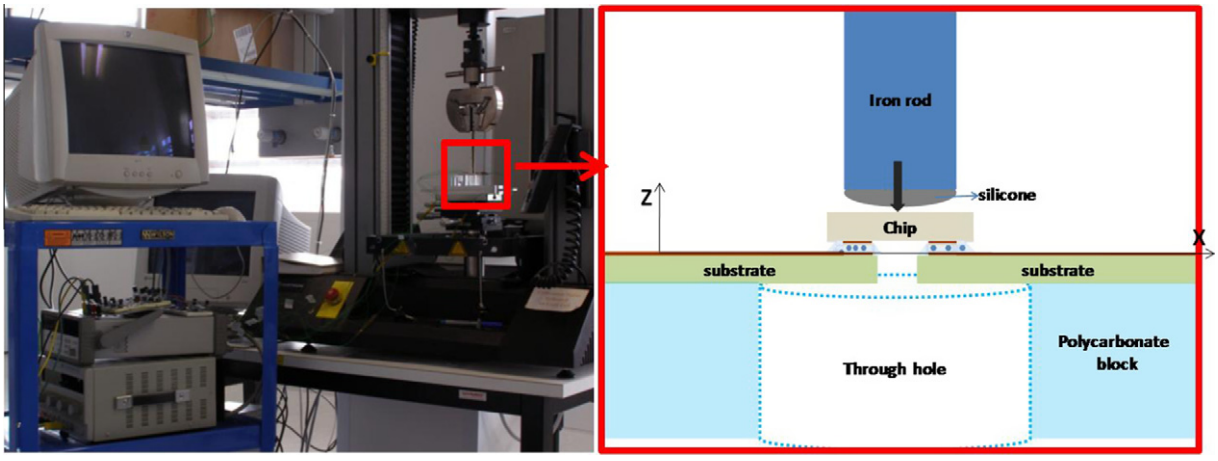

Fig. 7. Instron mechanical test setup and electrical test setup for testing ACA joints.

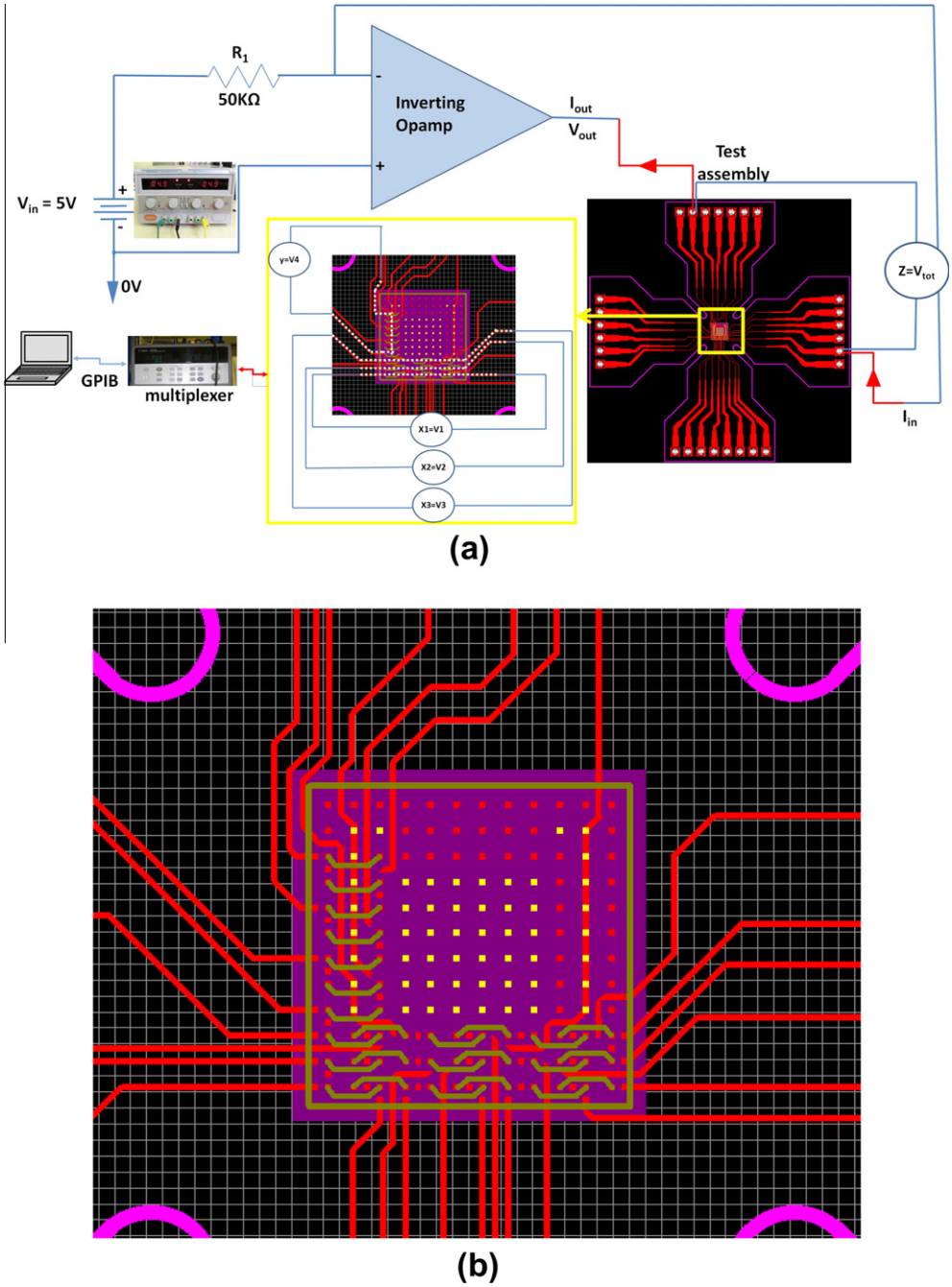

Fig. 8. (a) Schematic of the four point measurement test setup during mechanical test; and (b) layout showing the daisy chain in the test assembly.

An electrical circuit was made to make sure that it supplied 100 μA to the test assembly. A Digimess HY3003 power supply, set to deliver ±5 V, was connected to a 50 kΩ resistor which was connected in series with the negative input of an operational amplifier OP177. The positive input of the operational amplifier was connected to the ground of the Digimess HY3003. This setup allowed for 100 μA to be obtained at the operational amplifier output which would be supplied to the test assemblies. All the voltage measurements from the individual daisy chains and the total daisy chain were transmitted to the computer via GPIB. LabView was used to automate the measurements and the data was collected with an Agilent 349901A 20 channel multiplexer and recorded into Microsoft Excel. The test was carried out for 800 s and the electrical data was recorded every 5 s.

3. Results and discussion

In Fig. 9a, the primary axis represents the variation of the force with respect to the distance travelled by the ACA assembly in each diameter hole. The secondary axis shows the variation of the voltage measured in the total daisy chain of an ACA assembly as the sample was pushed through different diameter holes. An analysis of the insertion force curve in the 23 mm diameter hole will be used to explain the general form of the force curve obtained in other diameter holes. The general form of the force curve consisted of an initial linear part which corresponds to preliminary insertion of the assembly into the hole. This was characterised by the slow folding of the flex assembly's arms into a conical form as it is pushed through the hole. In this linear region the flex assembly

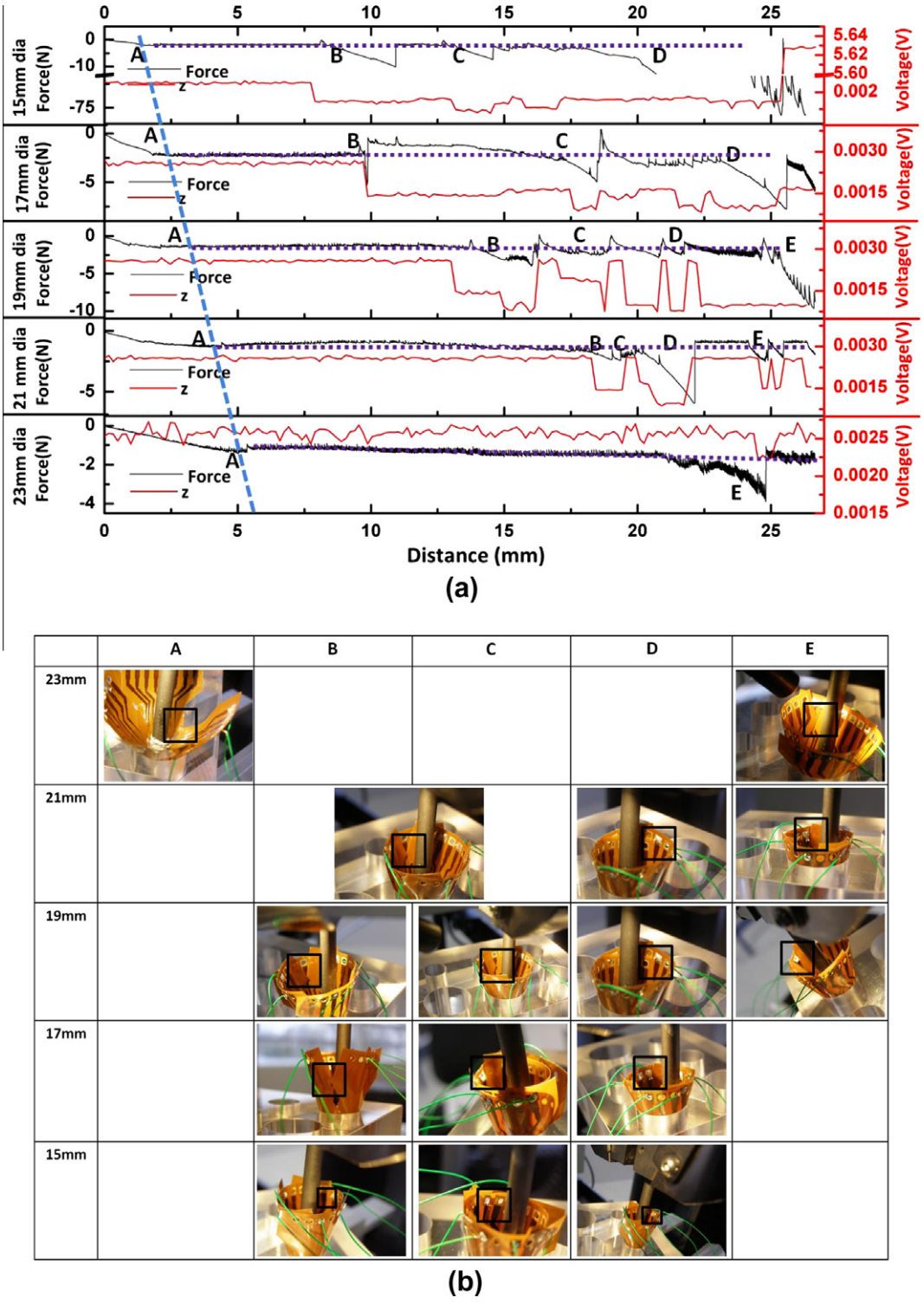

Fig. 9. (a) Plot showing the variation of the force and the measured voltage as a function of distance; and (b) images of the corresponding positions depicted in the force plot in different regions.

acts as a spring and opposes the assembly being pushed through the hole. Therefore this region could be approximated by Hooke's Law in the form:

$$F = -kd \tag{1}$$

where k (N/mm) is the spring constant, F is the force and d is the distance.

Fig. 10 shows the linear part of the force curve in the 23 mm diameter hole until position A. The slope of the linear part provided the spring constant and for 23 mm it was −0.2729 N/mm. At position A, the side corners of the extended arms of the flex cross of the fanned out region, close to the slit came in contact with each other, as shown in Fig. 9b. This corresponds to the end of the linear region where the assembly had folded into a conical form into the hole. From this point forward, there was no spring reaction from the

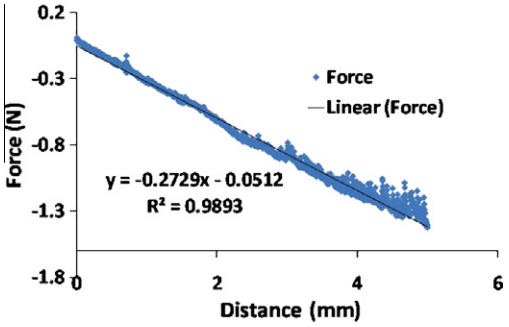

Fig. 10. Plot showing the linear part of the force curve in a 23 mm diameter hole until position A.

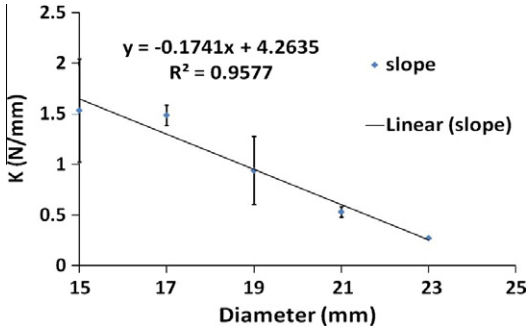

Fig. 11. Spring constant as a function of the hole diameter.

assembly and the only force encountered by the assembly was the friction from the side walls of the hole. As the surface of the side walls were polished little friction was experienced by the assembly when pushed through the hole. This could be approximated by a horizontal straight line until the end of the test. This constant force to push the assembly was disrupted by the corners of the extended arms entangling at around position E as shown in Fig. 9b. As soon as the arms slipped over each other, the force applied returned to its original constant value until the end of the insertion test.

Fig. 11 shows the spring constant k calculated from the slope of the linear part of the graph in Fig. 9a as a function of the hole diameter. It can be seen that the spring constant decreased linearly as the hole diameter was increased. This signifies that for the same distance, less force would be required in a larger diameter hole.

The conical shape occured at an earlier stage as the diameter of the hole shrank. This also led to the entanglement of the extended flex side arms at an earlier stage. This was indicated by positions B and C as shown in Fig. 9a and b. Further curling of the assembly onto itself led to one of the tips of the fanned out arms being caught up with its neighbouring soldered bond pad as shown in Fig. 9b, positions D and E. In the 15 mm diameter hole, this was apparent by the chip break which occurred at an insertion force of around 70 N.

The electrical response of the total daisy chain during insertion into the 23 mm diameter hole was characterised by a constant voltage except at around position E where there was a 15% drop in the measured voltage. This drop in the measured voltage was only momentary, i.e. after position E the voltage returned to its original value and corresponded to the increase in the force at position E. In 21 mm, 19 mm, 17 mm, and 15 mm diameter holes at position B and C, the average decrease in the measured voltage was around 44%, 53%, 46%, and 44%. A step decrease in the measured voltage was also observed for assemblies pushed through 19 mm, 17 mm and 15 mm diameter holes corresponding to positions B and C. This step-wise reduction in the measured voltage in the total daisy chain will be explained in detail when dealing with the partial daisy chains.

Table 1 shows the mechanical properties of the materials involved in the test. As mentioned earlier, an iron rod was placed on the back of the chip and pushed the assembly through the hole. This would generate stress on the chip, the flexible substrate and the adhesive that holds the chip and the substrate together. Since the assembly is pushed through, the stresses generated on the chip and the substrate are compressive and tensile in nature respectively [15]. As the elastic modulus of the chip is much greater than that of the flexible substrate, it will not bend as much as the substrate. Due to the relatively low elastic modulus of the ACA, it will tend to compress or deform in-between the chip and the substrate [15]. As a consequence the increased pressure on the back of the chip will be reflected by further compression of the joints.

The momentary decrease in the measured voltage was followed by it returning to its original value as soon as the applied force decreased or recovered to its initial values. As the entanglement passed through, the brief compression exerted on the joint was relaxed. During this brief compression, the conductive particles undergo elastic deformation and thus increase the contact area [24,25]. This would explain the decrease in the measured voltage which recovered at position E during insertion.

Fig. 12 shows the variation of the measured voltage in each partial daisy chain with respect to the distance travelled by the assembly as the mechanical test was carried out. For the partial daisy chains situated in the x axis, $x1$ and $x2$ which are located further away from the window showed no variation in the measured voltage while $x3$ close to the window showed a temporary 50% decrease in the measured voltage at a depth of 25 mm before returning to its original value. As stated in the previous section, the average decrease in the total daisy chain voltage was approximately 15%. This decrease corresponded to the increase in the force applied to the assembly, corresponding to position E as shown in Fig. 9a and b. Furthermore, the decrease in the measured voltage in the total daisy chain and the partial daisy chain happened at the same time. This was in perfect agreement with the result observed for the total daisy chain as it was just an addition of all the partial daisy chains. No decrease was observed on the partial daisy y situated close to the window in the y axis. At the end of the insertion test all the measured voltage values remained at or regained their original value, thus suggesting that in a capsule insertion the joint would not be under stress during further processing.

Since the rod was placed in the centre of the back of the chip during insertion, the maximum stress would be expected at the middle of the chip close to the window area [15]. Fig. 13 shows that for an assembly pushed through a cylindrical hole, the flexible substrate bend was limited by the slits made for facilitating the folding of the substrate during the insertion. As the full bend was not achieved, the adhesive holding the chip and the substrate at the chip perimeter would not be under high shear stress, as indicated in Fig. 13. The high stress region for this assembly would be at the flip chip end of the window opening where the chip was interconnected with the substrate. At position E, where the edge of the flex arm was entangled with the solder connector bond pad, as shown in Fig. 9b, the ACA would not compress uniformly from the window opening to the edge of the chip. Instead, the compression was greater at the window opening close to the centre of the chip than at the edge of the chip because of this. This would be the reason that the momentary increase in force observed at a depth of around 25 mm (position E) into the hole was reflected by a corresponding decrease in the measured voltage at the partial daisy chain $x3$, close to the window.

Fig. 14 shows the variation of the measured voltage in the individual partial daisy chains with respect to the distance travelled by

Table 1
Material parameters of the materials used in the mechanical test. Collected from [22,23].

Properties	ACA	PI flex	Chip
Young's modulus, E (MPa)	5900	4826	131,700
Poisson's ratio, v	0.3	0.3	0.3

the assembly as the mechanical test was carried out in 21 mm, 19 mm, 17 mm and 15 mm diameter holes. In order to observe the contribution clearly from individual daisy chains, the plots have been offset. As can be seen in Fig. 9a, the step like behaviour observed in the total daisy chain in the 19 mm diameter hole could be explained by the addition of the decrease observed in each partial daisy chain. For instance daisy chain $x3$ and y (closest to the window) showed an earlier sign of decrease in the measured voltage at around 14 mm of insertion into the hole. These had a percentage decrease of around 86% and 78% respectively. This as mentioned earlier, was due to the applied force on the back of the chip that resulted in the compression of the ACA joint. This decrease in $x3$ and y was responsible for the initial lowering of the total daisy chain voltage. The partial daisy chains $x1$ and $x2$ had a voltage decrease of about 88% and 90% at a depth of around 15 mm. As seen in Fig. 14, the decrease in the daisy chains $x1$ and $x2$ further away from the window occurred on top of the reduction that was already observed in $x3$ and y. This induced an additional reduction in the measured voltage, thus resulting in a step like behaviour observed in the total daisy chain.

The major information to be gathered from these graphs is the fact that, as the diameter of the hole decreased, due to the increased applied force to counterbalance the wall friction and mechanical contact, the measured voltage from the joints decreased. Another crucial piece of information to be gathered was that this voltage reduction was first observed in the partial daisy chains $x3$ and y that were closer to the window. For example, going through the graphs in descending order, i.e. from a 23 mm diameter hole to a 15 mm diameter hole, it can be noticed that the first reduction in the measured voltage always occurred at the partial daisy chains $x3$ and y which are closest to the window. It was also clear that as the diameter was reduced, the depth at which the voltage reduction occurred also reduced. It should be noted that as the hole diameter decreased, the measured voltage in these daisy chains did not return to their normal value until an open circuit was obtained at the 15 mm diameter insertion due to the die cracking. As the diameter decreased, the drop in the measured value in the daisy chains $x1$ and $x2$ (further away from the window) experienced more compression on the joints due to the higher force required to overcome the mechanical contact. Once again these measurements help to confirm the hypothesis that there was a high compressive stress on the chip close to the window joints and that this could be used as a design consideration for further designing of interconnection for capsule integration. Although, going for a wider diameter hole would produce less strain on the joints, in this research the limit was set to 23 mm diameter hole so that it represented twice the size of a standard capsule.

Fig. 15a shows the micrograph of the assembly after the open circuit occurred. The cracks seem to widen near the centre of the chip and also close to the void that was present in the ACA, thus implying that it started simultaneously at the centre and at the corner of the chip and that the stress was high in these regions. The right hand micrograph in Fig. 15b shows an image of another cracked die. It can be seen that the silicon die at the centre seemed to have lifted and there is a slight depression close to the edge of the window. It can also be noticed that the cracks seem to widen

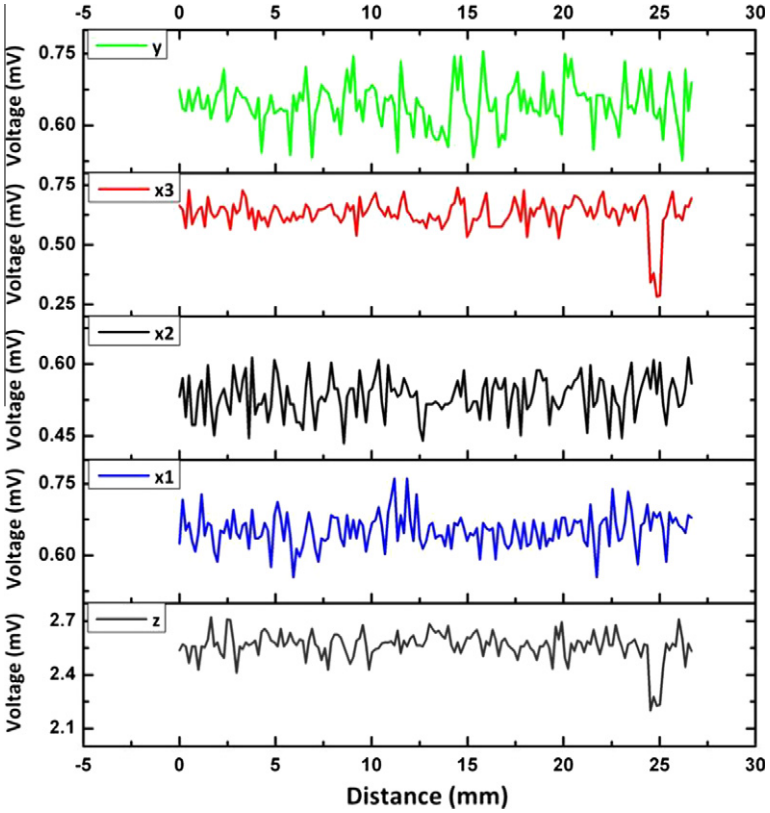

Fig. 12. Variation of the measured voltage as a function of the distance travelled in a 23 mm diameter hole.

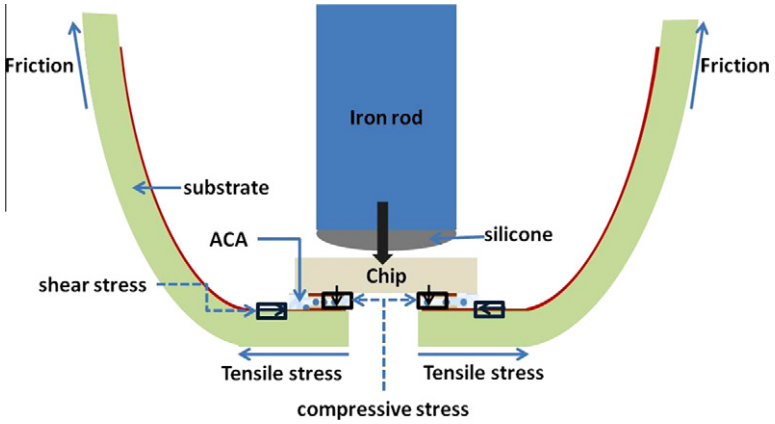

Fig. 13. Schematic showing the regions of stress in the assembly during insertion.

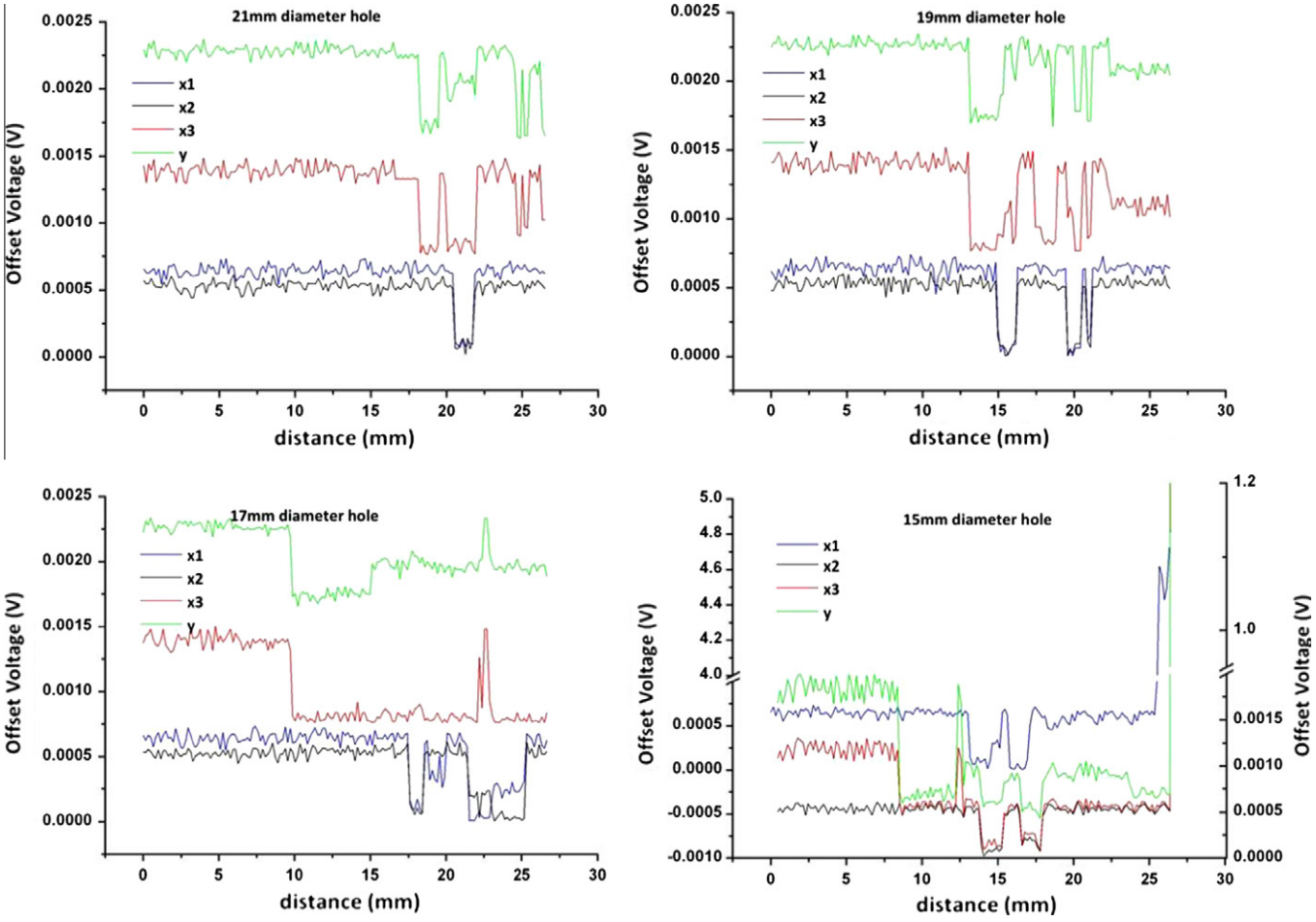

Fig. 14. Plot showing variation of voltage in each individual daisy chain as a function of distance travelled in 21 mm, 19 mm, 17 mm, and 15 mm diameter holes.

at the point where the silicon die seemed to lift off. The depression and the wide crack close to the window imply that the stress was high in this region. On both micrographs, the silver regions represent the surface chipping of the silicon die. The maximum load that the silicon test die could withstand in compression was around 70 N. This was in accordance with the finding that a die of thickness of around 0.4 mm would require a break load of about 70 N [26].

An analysis of the failed ACA contacts after the mechanical test was carried out by cross-sectional analysis. Fig. 16 shows the cross-sectional micrograph of one of the flip chip ACA contacts. Fig. 17 shows the position where the cross-sectional micrograph was taken.

It can be noticed from Fig. 16a, that the crack was wide close to the bump and the crack width gradually decreased towards the top of the silicon chip. From Figs. 16b and 17, it could be noticed that

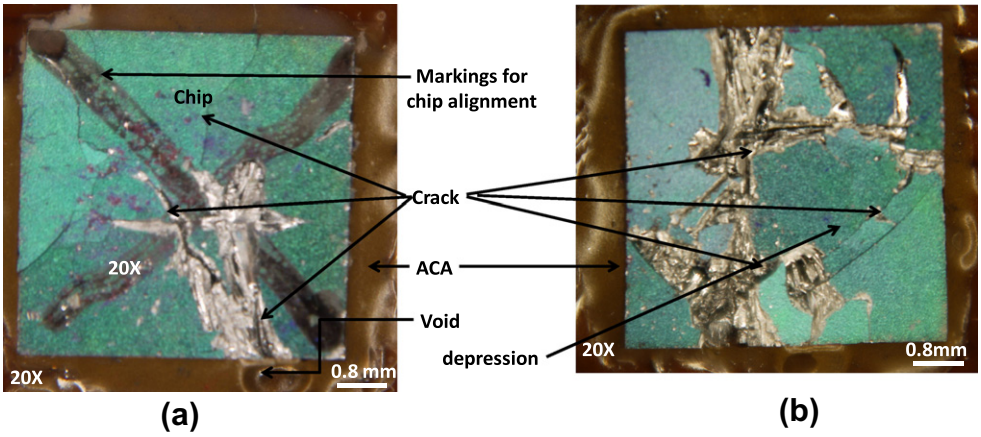

Fig. 15. Micrographs showing the cracked die after mechanical testing.

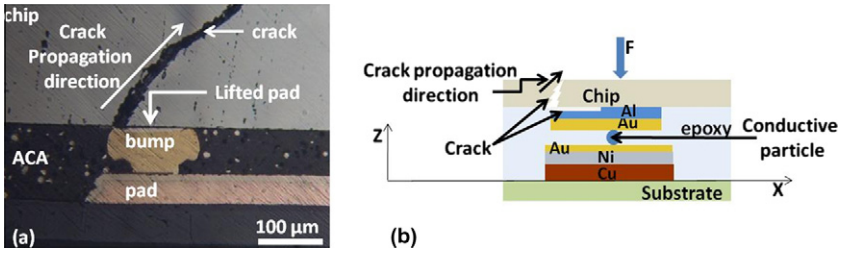

Fig. 16. (a) Cross sectional micrograph showing the crack propagation in the ACA assembly and; (b) schematic of the cross section showing force and direction of propagation.

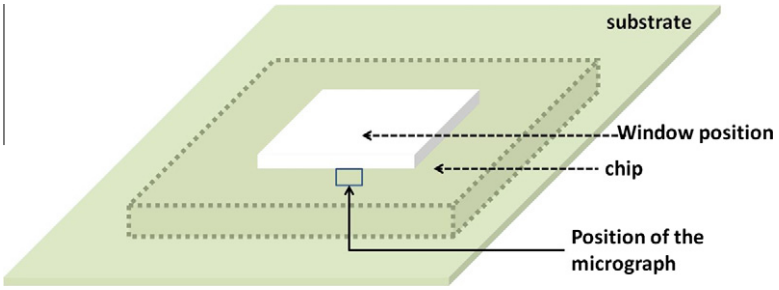

Fig. 17. Schematic showing the position of the cross-section micrograph.

the bond pad was close to the applied force and that the crack was oriented towards the applied force. It also suggests that the stress was high close to the edge of the window and that the stress was built up in the epoxy from where it was released by die cracking and pad lift off. It could also be noticed that the ACA adhesion to the substrate was still strong with a good contact with the ACA conductive particle. This may be the reason why the $x1$ and $x2$ resistance showed a sudden open contact. This showed that the weakness was on the chip pad side and not on the ACA contact.

4. Conclusion

This study has described the mechanical reliability testing of an ACA joint during the insertion of a flex test assembly into different diameter holes representing different capsule diameters. The insertion test described in this paper is similar to an inward bend test and can be characterised by the die positioned on the positive side of the z axis. During insertion into the holes, the force curve was characterised by a linear region and a constant region characterised by the low friction of the assembly. The flex assembly acted as a spring and opposed the assembly being pushed through the diameter hole and was approximated using Hooke's law. The spring constant for the 23 mm diameter hole assembly was 0.2729 N/mm and increased to 1.5 N/mm for the 15 mm diameter hole. The spring constant decreased linearly with increasing hole diameter signifying that for the same distance, less force will be required in a larger diameter hole. After the initial linear insertion, further pushing through the hole was characterised by a constant force. The flex assembly deformed into a conical shape at an earlier stage as the diameter of the hole decreased. This also caused the entangling of the extended flex side arms to occur at an earlier stage. The electrical measurement in the total daisy chain made during insertion closely matched the insertion force, i.e. every increase in the insertion force was matched by a corresponding decrease in the measured voltage.

During insertion the stress in the assembly was higher towards the centre of the chip and the window than at the edge of the chip and the ACA fillet. This was demonstrated by the lower voltage values measured in the partial daisy chains that were close to the

window rather than those that were situated away from the window. In these daisy chains, as the hole diameter was reduced, the insertion depth at which the voltage reduction occurred also reduced, and the measured voltage did not return to its original value until an open circuit was obtained. It also showed that a high compressive stress was applied to the middle of the chip and close to the window compared to the edge of the chip and the ACA fillet.

This mechanical test and the electrical measurements throughout the insertion test suggested that the 23 mm diameter hole would be the smallest suitable hole for insertion of this assembly. This implies that a capsule diameter of 23 mm was the smallest that could be used in the DAS integration process for this specific substrate and chip design.

Failure analysis showed that cracks could be noticed close to the centre of the chip while smaller cracks were visible close to the edges of the chip, suggesting high stress close to the centre of the chip. The cross-sectional analysis showed that the failure occurred within the silicon/silicon chip pad and that the ACA contacts formed a strong joint and were able to withstand the insertion force required to secure the ACA sensor in place before encapsulation.

Future work will involve finite element analysis of the structure and a comparison with the results presented in this paper.

References

[1] Cumming DR, Hammond PA, Wang L. Wireless endoscopy: technology and design, microengineering in biotechnology, methods in molecular biology. In: Hughes MP, Hoettges KF, editors. Microeng Biotechnol, vol. 583. New Jersey: Springer Protocols; 2008. p. 221–46.

[2] McCaffrey C, Chevalerias O, O'Mathuna C, Twomey K. Swallowable-capsule technology. IEEE Pervasive Comput 2008;7:23–9.

[3] Costamagna G, Shah S, Riccioni M, Foschia F, Mutignani M, Perri V, et al. A prospective trial comparing small bowel radiographs and video capsule endoscopy for suspected small bowel disease. Gastroenterology 2002;123:999–1005.

[4] Twomey K, Marchesi J. Swallowable capsule technology: current perspectives and future directions. Endoscopy 2009;41:357–62.

[5] Philips Intellicap Technology, available at: <http://www.research.philips.com/newscenter/backgrounders/081111-ipill.html>.

[6] Allan R. Smart pill goes on a fantastic voyage. Electron Des 2006;54:27–66.

[7] Dettmer R. Fantastic voyage [wireless capsule endoscopes]. IEEE Review 2004;51:28–32.

[8] Wang L, Johannessen E, Hammond P, Cui L, Reid S, Cooper J, et al. A programmable microsystem using system-on-chip for real-time biotelemetry. IEEE Trans Biomed Eng 2005;52:1251–60.

[9] Cooper J, Johannessen E, Cumming D. Bridging the gap between micro and nanotechnology: using lab-on-a-chip to enable nanosensors for genomics, proteomics, and diagnostic screening. Netw Parall Comput 2004:517–21.

[10] Johannessen E, Wang L, Reid S, Cumming D, Cooper J. Implementation of radio telemetry in a lab-in-a-pill format. Lab Chip 2006;6:39–45.

[11] Johannessen E, Wang L, Cui L, Tang T, Ahmadian M, Astaras A, et al. Implementation of multichannel sensors for remote biomedical measurements in a microsystems format. IEEE Trans Biomed Eng 2004;51:525.

[12] Tang T, Johannessen E, Wang L, Astaras A, Ahmadian M, Murray A, et al. Toward a miniature wireless integrated multisensor microsystem for industrial and biomedical applications. IEEE Sens J 2002;2:628–35.

[13] Briegel R, Ashauer M, Ashauer H, Sandmaier H, Lang W. Anisotropic conductive adhesion of microsensors applied in the instance of a low pressure sensor. Sens Actuators A 2002;97–98:323–8.

[14] Jesudoss P, Mathewson A, Wright W, McCaffrey C, Ogurtsov V, Twomey K, et al. System packaging and integration for a swallowable capsule using a direct access sensor. In: IEEE microelectronics and packaging conference, EMPC; 2009. p. 1–4.

[15] Rizvi M, Chan Y, Bailey C, Lu H. Study of anisotropic conductive adhesive joint behavior under 3-point bending. Microelectron Reliab 2005;45:589–96.

[16] Yip MC, Huang CY, Chen CL, Lu ST. Bending and reliability test of chip-on-flex (COF) assembly using anisotropic conductive films (ACFs). In: Eighth international conference on electronic packaging technology; 2007. p. 1–3.

[17] Noh BI, Yoon JW, Kim JW, Lee JB, Park NC, Hong WS, et al. Reliability of Au bump flip chip packages with adhesive materials using four-point bending test. Int J Adhes Adhes 2009;29:650–5.

[18] Lu ST, Chen WH. Reliability of ultra-thin chip-on-flex (UTCOF) with anisotropic conductive adhesive (ACA) joints. In: 58th Electronic components and technology conference; 2008. p. 1287–93.

[19] Lu ST, Chen WH. Reliability and flexibility of ultra-thin chip-on-flex (UTCOF) interconnects with anisotropic conductive adhesive (ACA) joints. Adv Pack IEEE Trans 2010;33:702–12.

[20] Cai XH, An B, Lai XW, Wu YP, Wu FS. Reliability evaluation on flexible RFID Tag inlay packaged by anisotropic conductive adhesive. In: Eighth international conference on electronic packaging technology, ICEPT; 2007. p. 1–4.

[21] An B, Cai XH, Chu HB, Lai XW, Wu FS, Wu YP. Flex reliability of RFID inlays assembled by anisotropic conductive adhesive. In: High density packaging and microsystem integration HDP '07, international symposium; 2007. p. 1–4.

[22] Islam R, Chan YC, Ralph B. Effect of drop impact energy on contact resistance of anisotropic conductive adhesive film joints. J Mater Res 2004:1662–8.

[23] Seppälä A, Ristolainen E. Study of adhesive flip chip bonding process and failure mechanisms of ACA joints. Microelectron Reliab 2004:639–48.

[24] Kwon WS, Paik KW. Experimental analysis of mechanical and electrical characteristics of metal-coated conductive spheres for anisotropic conductive adhesives (ACAs) interconnection. IEEE Trans Compon Packag Technol 2006:528–34.

[25] Duraj A, Mach P. Analysis and prediction of electrical contact resistance for anisotropic conductive adhesives. In: 31st International spring seminar on electronics technology; 2008. p. 358–62.

[26] Chong DYR, Lee WE, Lim BK, Pang JHL, Low TH. Mechanical characterization in failure strength of silicon dice. In: The ninth intersociety conference on thermal and thermomechanical phenomena in electronic systems; 2004. p. 203–10.